Mechanical Systems and Signal Processing 228 (2025) 112465

Contents lists available at ScienceDirect

Mechanical Systems and Signal Processing

journal homepage: www.elsevier.com/locate/ymssp

Noncontact elastography of soft material using a laser profilometer with airpuff excitation

Xiao Chen [a], Yichu Chen [a], Wei Yu [a], Sanming Hu [a], Pengcheng Li [b,*]

[a] School of Biomedical Engineering and Imaging, Xianning Medical College, Hubei University of Science and Technology, Xianning, 437100, Hubei, China
[b] State Key Laboratory of Digital Medical Engineering, Key Laboratory of Biomedical Engineering of Hainan Province, School of Biomedical Engineering, Sanya, 572025, Hainan, China

ARTICLE INFO

Communicated by J. Rodellar

Keywords:
Laser profilometer
Soft material characterization
Surface wave
Noncontact elastography

ABSTRACT

Elasticity is a fundamental property of materials, and recent advancements in wave-based elastography have revealed significant potential for various biomedical and engineering applications, including biomedical imaging, nondestructive evaluation, and structural health monitoring. However, the implementation of elastography requires high-precision imaging systems, which limits its broader applicability. The laser profilometer, a conventional and cost-effective device that operates based on laser triangulation measurement, has been widely utilized in industrial applications for assessing surface profiles. However, its application in elastography has not been previously explored. This study represents, to the best of our knowledge, the first attempt to adapt a laser profilometer for measuring the elasticity of soft materials. A simple and noncontact method for measuring elasticity has been established utilizing the laser profilometer to track the propagation of surface waves on soft materials when excited by an airpuff. The results demonstrate that laser profilometer elastography can track the propagation of surface waves with a broad spectrum following a single airpuff excitation. The temporal separation of wave propagation from the reflected waves enables precise calculation of the propagation velocity of surface waves. The surface wave velocities measured by laser profilometer elastography and laser speckle elastography show strong agreement with a correlation coefficient of 0.997. Additionally, the shear elastic modulus of agarose phantoms has been validated by comparing the results obtained from a rotary rheometer. This approach improves the noncontact elastic measurement capabilities of traditional laser profilometers by only utilizing an airpuff system. Therefore, it has the potential to expand a new application of laser profilometers and be widely utilized for elasticity measurement in both biomedical and industrial applications.

1. Introduction

Elasticity is a fundamental property of materials [1,2]. The measurement of elasticity has extensive applications in both industrial fields [3–6] and biomedical applications [2,7–12], including nondestructive evaluation, structural health monitoring, and biomedical imaging [4]. However, traditional devices for measuring elasticity, such as rotational rheometers, tensile testers and dynamic mechanical analyzers tend to be rigid, bulky and expensive [7]. In contrast, novel elastography technologies offer advantages, such as

---

* Corresponding author.
E-mail address: pengchengli@hainanu.edu.cn (P. Li).

https://doi.org/10.1016/j.ymssp.2025.112465
Received 27 November 2024; Received in revised form 23 January 2025; Accepted 10 February 2025

noncontact measurement and no requirement for standard sample, which have attracted significant attention. Emerging elastography methods, based on ultrasound imaging [11], optical coherence tomography (OCT) [2,9,10,12–15], photoacoustic imaging [16,17], optical holography [18], laser speckle imaging (LSI) [19–22] and laser Doppler vibrometer (LDV) [3,4], have made significant advancements. Particularly in biomedicine, the elasticity of tissues can provide valuable insights into their physiological and pathological states, making it useful for disease diagnosis [7,18]. Elastography has been employed in diagnosing skin diseases [13], assessing hepatic dysfunction [11] and quantifying corneal condition [9,14].

Recent developments have led to the emergence of characterization methods grounded in wave propagation to measure the elastic properties of soft materials. Wave-based elastography is critical for both nondestructive evaluation [3–6,23] and biomedical applications [2,9,11–18,21,22,24]. Ghaderi et al. presented a method for characterizing soft material through surface wave elastography using a LDV with consecutive pulses of air excitation [3]. Cai et al. focused on developing a piezo stack-LDV sensing approach for characterizing shear wave dispersion and local viscoelastic properties [4]. A novel wearable bioadhesive ultrasound elastography was developed for continuous monitoring of modulus changes during the rapid development of hepatic dysfunction in rat liver [11]. Singh et al. proposed integrating reverberant shear wave fields with OCT for high resolution elastography at different developmental stages of murine embryos [12]. Moon et al. demonstrated the utilization of high-frequency optical coherence elastography (OCE) for characterizing gingival tissue in both porcine models and human subjects [15]. Wang et al. introduced an OCE method incorporating homolateral parallel acoustic radiation force excitation for measuring the elasticity of the ocular tissues [14]. Singh et al. reported on quantifying viscoelastic parameters by tracking Rayleigh waves using holographic imaging [18]. Liu et al. presented a photoacoustic elastography based on laser-excited shear waves [16]. Our group also reported simultaneous measurements of viscosity and elasticity using laser speckle contrast imaging (LSCI) [22].

However, elastography methods based on elastic waves (such as shear wave and surface wave) need to track the rapid propagation of elastic waves. This necessitates imaging techniques with high sampling rates and precise detection capabilities. In ultrasound shear wave elastography, the implementation of planar wave imaging methods is essential for achieving imaging frame rates of up to several thousand frames per second [11]. In OCE, it is essential for the system to achieve a high-speed A-line scanning rate which is typically facilitated by incorporating a high-speed swept laser source [9,14,15] or a high-speed spectrometer [12,24]. For wide-field imaging methods, such as LSI and optical holography, the utilization of high-speed cameras is essential for attaining critical frame rates that exceed several thousand frames per second [18]. LDV exhibits high sensitivity in velocity measurement, which makes light work of vibration measurement [25]. Additionally, LDV has been employed in elastography, requiring high-speed LDV systems [3,4]. Current elastography techniques require acquisition systems with specialized high precision and rapid sampling rates. However, the high-cost and complexity of elastography systems limit their application and widespread adoption [10].

Several methodologies have been proposed to reduce the performance demands of imaging systems. Stroboscopy, or stroboscopic imaging, is a cost-effective approach commonly utilized to attain a high sampling rate [20,22,26]. Von Gierke et al. demonstrated the application of low-cost stroboscopic techniques for detecting surface waves induced by piston vibrations [26]. Additionally, our research group was the first to demonstrate elastography utilizing low-frame-rate LSCI by leveraging the aliasing effect [21]. Feng et al. introduced ultra-wideband optical coherence elastography to measure the stiffness of hard materials in conventionally inaccessible ranges upto 1 MHz by taking advantage of signal aliasing [2]. Schmidt et al. utilized the complete recovery of the harmonic shear wave field in an asynchronous, conventional frame-rate, raster-scanning OCT system [10]. The enhancement of system synchronization introduces additional complexity to the system, while interference arising from multiple excitations and the continuous reflection of wave fields can further complicate the wave dynamics, thereby impeding accurate velocity calculations.

Investigating novel elastography methods utilizing well-established commercial industrial inspection equipment represents a promising approach to developing simple elastic imaging systems and broadening the applications of elastic measurement. The laser profilometer, which operates based on laser triangulation measurement, has been widely utilized in both industrial and research settings for profile measurement, providing micron accuracy across a large measuring range. Its applications include measuring height profiles during laser melting experiments [27], assessing the vibrations of wind turbine blades [28], and conducting on-machine measurements of complex surfaces [29]. However, it has not yet been used for elastography.

Therefore, this article first presents the elastography utilizing a laser profilometer, thereby establishing a novel area of application for laser profilometer. A simple noncontact elastography method for soft material has been developed utilizing a commercially available laser profilometer. This method employs the laser profilometer to detect the vibration of the surface wave induced by airpuff excitations. Subsequently, the propagation velocity of the surface wave is calculated. Thanks to advancements in optoelectronic technology, current commercial laser profilometers can achieve line scanning speeds of several kilohertz, along with micrometer-level repeatability in the z-axis [29]. This capability makes them ideally suited for the elastic measurement of soft materials. The benefits of our proposed method include: (1) It expands the measurement capabilities of the laser profilometer from profile measurement to elastography; (2) The elastography system based on the laser profilometer is simple and cost-effective. Only an airpuff excitation system needs to be added to the existing commercial laser profilometer. Furthermore, elasticity can be measured using a single excitation. (3) Noncontact elastography measurement mitigates the risk of sample contamination during testing. Consequently, the elastography we present is advantageous for enhancing elastic measurement methodologies in both biomedical and industrial applications.

2. Methods

2.1. Surface wave elastography

For a homogeneous, isotropic, viscoelastic, and compressible medium, Navier's equation with zero equivalent body forces can be expressed as [30–32]:

$$(\lambda + 2\mu)\nabla\nabla \cdot \boldsymbol{u} - \mu\nabla \times \nabla \times \boldsymbol{u} = \rho \frac{\partial^2}{\partial t^2}\boldsymbol{u} \tag{1}$$

where, $\boldsymbol{u}$ is the displacement vector, ρ is the density of the medium, $\partial/\partial t$ denotes a derivative with respect to time t. $\nabla\cdot$ is the divergence operator, $\nabla\times$ is the curl operator, and ∇ is the gradient operator. λ and μ are the first and second Lamé constants of the medium. By applying the Stokes-Helmholtz decomposition theorem, compressional wave (P wave) and shear wave (S wave) can be calculated as [32]:

$$\nabla^2\varphi = \frac{1}{V_P^2}\frac{\partial^2}{\partial t^2}\varphi \tag{2}$$

$$\nabla^2\boldsymbol{\psi} = \frac{1}{V_S^2}\frac{\partial^2}{\partial t^2}\boldsymbol{\psi} \tag{3}$$

where, φ and $\boldsymbol{\psi}$ are the P and S wave potential functions respectively. The P wave velocity V_P is given by $V_P = \sqrt{(\lambda + 2\mu)/\rho}$, and the shear wave velocity V_S is expressed as $V_S = \sqrt{\mu/\rho}$.

The P wave and S wave superimpose under specific boundary conditions on the sample surface, resulting in the formation of surface waves, also known as Rayleigh waves (R waves). An analytical solution has been derived for Rayleigh wave propagation on the surface of an isotropic homogeneous viscoelastic half-space caused by a normal force [30,31]. In the context of elastography discussed in this paper, the primary focus is on the propagation velocity of elastic waves. The wave arriving at the location $\boldsymbol{x}$ can be expressed in a simplified manner as [33–35]:

$$u(t, \boldsymbol{x}) = Ae^{j[\omega t - \boldsymbol{k}\cdot(\boldsymbol{x}-\boldsymbol{p})]} \tag{4}$$

where, A is the amplitude of the surface wave, ω is the frequency in radians, $\boldsymbol{p}$ is the source location, and $\boldsymbol{k}$ is the wavenumber. For viscoelastic materials, both A and $\boldsymbol{k}$ are frequency dependent. The surface wave propagates away from the source with a phase velocity of $V_R = \omega/\boldsymbol{k}$ [36], and the amplitude decays by geometric spreading, scattering, and absorption.

The relationship between surface wave velocity and the shear wave velocity is $V_R = V_S(0.87 + 1.12\nu)/(1 + \nu)$, where ν is the Poisson's ratio of the material [33]. Additionally, the shear elastic modulus G can be calculated as $G = \rho V_S^2$. For viscous media, both V_S and V_R are complex values and frequency dependent. In the field of elastography, particularly concerning soft biological tissues or polymeric materials, it is commonly posited that the Poisson's ratio is approximately 0.5. The shear wave velocity can be related to the surface wave velocity as $V_S \approx 1.05V_R$ [33,37,38]. The shear elastic modulus G of soft materials can be related to V_R as [37]:

$$G = \rho(1.05V_R)^2 \tag{5}$$

Therefore, the elastic property of soft materials can be characterized by determining the surface wave velocity from the spatiotemporal distribution of displacements induced by surface wave vibration.

2.2. Elastography using laser profilometer

A laser profilometer was primarily utilized for measuring surface profiles. Thanks to advancements in miniature optics, advanced microelectronics, and signal pre-processing, compact laser profilometer systems are capable of measuring surface profiles automatically, rapidly, and accurately, which is expected to be used for tracking the spatiotemporal distribution of displacement to calculate the elasticity of samples.

Fig. 1(a) is the schematic of the noncontact elastography utilizing a laser profilometer with airpuff excitation. The system consists of two parts: excitation and detection. Control signals for the solenoid valve and the triggering signals for the profilometer are generated by a data acquisition (DAQ) card controlled by custom-made software. High-pressure gas generated by the air pump is adjusted to the desired pressure range using a pressure regulator and then connected to the solenoid valve.

The instantaneous interruption of the solenoid valve results in generating a high-pressure pulse of airflow, which is expelled through a nozzle directed at the surface of the phantom. When the sample is disturbed by the force exerted by an airpuff, a surface wave is generated. The distribution of spatiotemporal displacements of the surface wave can be tracked using a laser profilometer (labeled as a gray box). The sensor head emits a blue laser beam that illuminates the phantom. After being reflected by the phantom's surface, the laser beam is directed onto an optical sensor through a lens within the profilometer's head. Fig. 1(b) illustrates the principle of displacement measurement using the laser triangulation method. The laser profilometer operates on the triangulation principle to convert the measured displacement y into positional changes x of the light on the sensor [29]. Most commercial laser profilometers have integrated calculation functions that enable the direct output of displacement values.

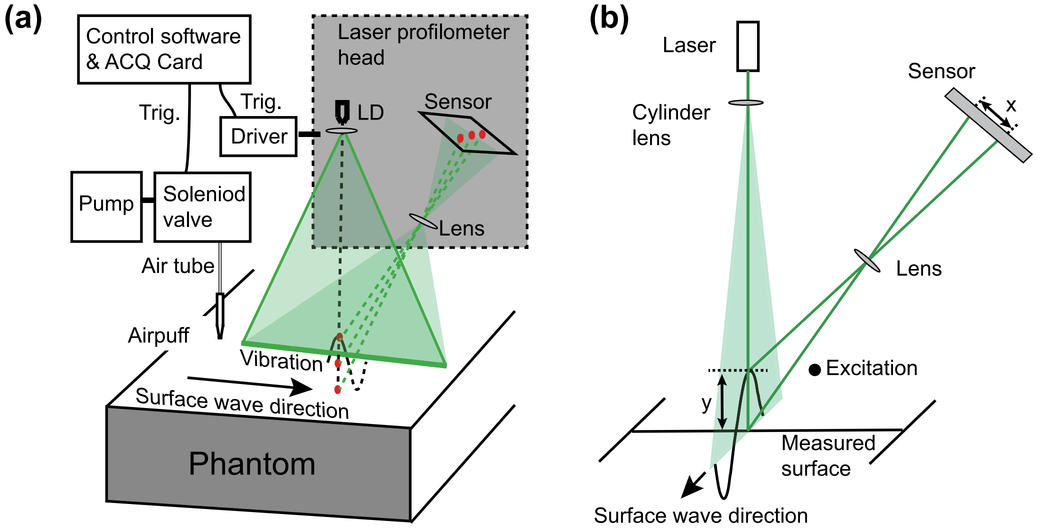

Fig. 1. Principle of elastography utilizing a laser profilometer. (a) Schematic of noncontact elastography using a laser profilometer with airpuff excitation. (b) Principle of displacement measurement using a laser triangulation method.

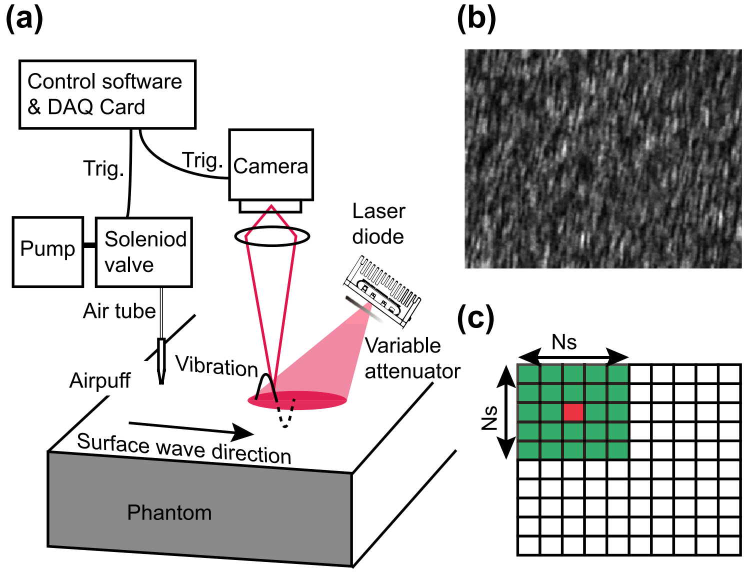

Fig. 2. Principle of elastography utilizing LSCI. (a) Schematic of noncontact elastography using LSCI with airpuff excitation. (b) Speckle imaging of a moving paper under laser illumination. (c) Schematic of speckle contrast calculation within a moving window.

2.3. *Elastography using laser speckle contrast imaging*

To verify the accuracy of elastic measurements, a comparative analysis was conducted with surface wave velocities measured by reflective speckle elastography. Fig. 2(a) illustrates a schematic of the noncontact elastography using LSCI with airpuff excitation. The airpuff excitation system employed is identical to that utilized in laser profilometer elastography. While the spatiotemporal distribution of the surface wave is tracked using LSCI. The LSCI detects fluctuations in speckle patterns caused by the random scattering of particles, shown in Fig. 2(b). The surface wave propagation modulates the scattering particles, which causes the speckle contrast to decrease. As shown in Fig. 2(c), The speckle contrast C is defined as the ratio of the standard deviation σ to the mean intensity $\langle I \rangle$ within a local window of pixels with size of Ns:

$$C = \frac{\sigma}{\langle I \rangle} \tag{6}$$

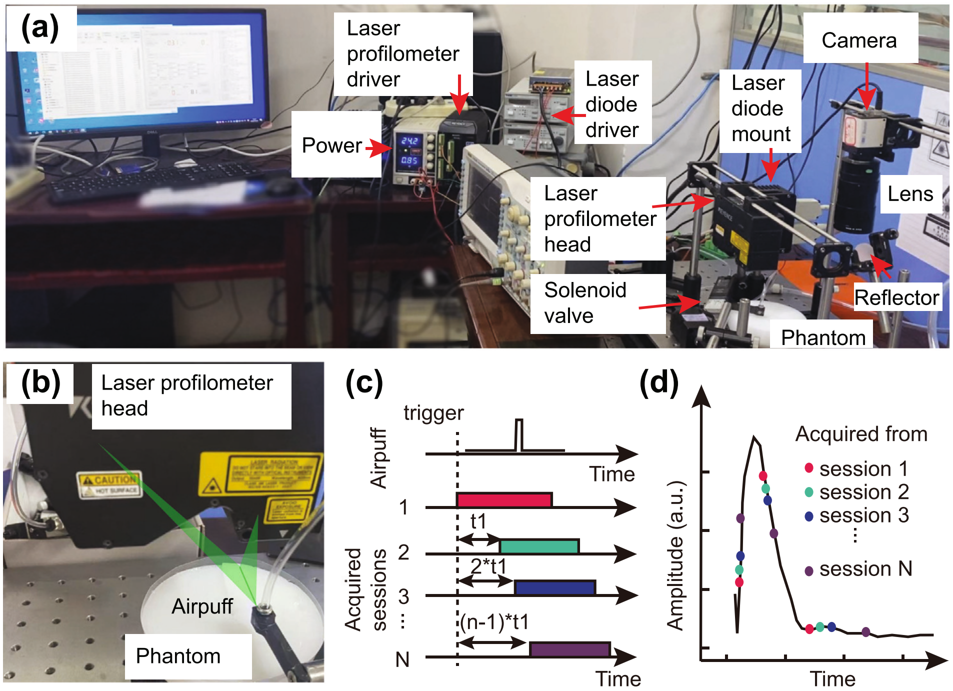

Fig. 3. Experimental setup for laser profilometer elastography and laser speckle elastography. (a) Photograph of the experimental setup. (b) Close view of the laser profilometer elastography, phantom setup, and airpuff. A schematic showing the stroboscopic imaging (c) timing sequence and (d) corresponding data acquired.

The speckle contrast map indicates the propagation of the surface wave within the spatiotemporal domain. The propagation velocity of the Rayleigh wave is consistent with that of the speckle contrast field. The accuracy of elastography using LSCI has been fully validated by prior researches [20–22].

3. Experimental setup

To validate the feasibility of elastography using a laser profilometer, we conducted experiments on agarose tissue-mimicking phantoms. The surface wave velocity, measured by the laser profilometer and LSCI, was subjected to comparative analysis. Fig. 3(a) presents a photograph of the experimental setup utilized for both laser profilometer elastography and laser speckle elastography. This setup illustrates the integration of a solenoid valve, an agarose phantom, a laser profilometer device equipped with a head and driver, and an LSCI system that includes a laser diode (LD) driver, an LD mount, and a camera. Both elastography techniques utilize the same airpuff excitation system instead of employing different tracking methods, thereby facilitating a side-by-side comparison of the results.

To generate surface waves on the sample, an industrial solenoid valve (FESTO, MHJ10-S-0.35-QS-4-MF) was utilized. This valve was connected to an adjustable precision pressure regulator (DELIXI, IR1020-01BG) to regulate the air pressure to approximately 2 bar (200 kPa). The incorporation of a nozzle enhanced the airflow by converting it into a more laminar and focused stream, thereby ensuring the precise application of force at a designated location on the specimen.

3.1. Experiments for laser profilometer elastography

Fig. 3(b) illustrates a close-up view of the laser profilometer elastography setup. The laser profilometer head (KEYENCE, LJ-V7060) emits a blue line laser beam with a length of 15 mm, which illuminates the phantom. The reflected laser beam is directed onto the optical sensor through a lens within the profilometer head. The schematic of the light path is indicated by a blue line. The measurement range of the profilometer head is 60 ± 8 mm along the z-axis, with a maximum line acquisition speed of 16 kHz. The nozzle is secured by a 3D-printed bracket and support rods. Prior to the acquirement of the experiment, the profilometer operates in preview mode, configured for internal triggering with a data acquisition rate of 200 Hz. A output measurement value is set at the middle position of the profile. In preview mode, the software provides real-time outputs of profile curves and corresponding height values, enabling the adjustment of the phantom surface height to approximately 0 mm. During the process of tracking surface waves, the profilometer is configured to operate in high-speed acquisition mode. The bin sizes for the x-axis and z-axis are set to 2 pixels, and the system utilizes external triggering, allowing for a maximum acquisition speed of 8 kHz. The profilometer head is driven by the controller (KEYENCE, LJ-V7001P). The controller facilitates communication with the computer for parameter configuration, status monitoring, and data transfer. Control signals for the solenoid valve and the triggering signals for the profilometer are managed by a DAQ card (ART, PCIe5654) after being converted to the 24 V voltage level.

To investigate the impact of sampling rate on the accuracy of elastic measurements and spatial resolution, we conducted experiments utilizing three different sampling rates to track the surface wave at 6.25 kHz, 20 kHz, and 50 kHz. Fig. 3(c) is a schematic representation of the timing sequence. The principle involves conducting multiple acquisitions with a time-lapse to capture different parts of the signal during each session, as shown in Fig. 3(d). The controller activates a solenoid valve to generate an 8 ms pulse excitation, and a laser profilometer is triggered in advance to collect a baseline value over 15 ms. For acquisition at 6.25 kHz, a series of pulses was generated with a period of 0.16 ms, corresponding to a frequency of 6.25 kHz. This sampling rate does not exceed the maximum sampling capability of the laser profilometer, enabling direct acquisition within a single excitation (N=1). For acquisitions at 20 kHz and 50 kHz, a stroboscopic imaging sequence was used. The laser profilometer operates at 6.25 kHz and repeats 8 times with a time delay of 0.02 ms, i.e. t1 = 0.02 ms and $N = 8$, to achieve an effective sampling rate of 50 kHz. The laser profilometer operates at 1 kHz and repeats 20 times with a time delay of 0.05 ms, i.e. t1=0.05 ms and N=20, to achieve an effective sampling rate of 20 kHz. In each experiment, a total of 2000 profiles were acquired with each profile containing 400 points. A custom-made control software featuring a graphical user interface was developed using C++ and the application programming interfaces provided by the profilometer and the DAQ card. The software is designed to automatically configure the laser profilometer, manage the DAQ card to conduct experiments using specific parameters, and save the acquired data to files once the predetermined number of profiles is reached.

3.2. Experiments for laser speckle elastography

In order to assess the accuracy of elastic measurement, a comparative analysis was conducted with the surface wave velocity measured by laser speckle elastography. The laser diode controller kit (Thorlabs, LTC56B) is utilized to drive the LD (Sharp,GH0782RA2C), which emits a laser with a wavelength of 780 nm that illuminates the sample. A camera (Baumer, TXG14f) captures scattered light through a zoom lens. To improve the acquisition frame rate of the camera, a bin size of 2 × 2 pixels is employed. This configuration allows for image acquisition at a resolution of 480 × 240 pixels, maintaining a fixed frame rate of 200 Hz with an exposure time of 0.5 ms. The acquisition process is conducted in 100 sessions, with a delay of 0.05 ms between each acquired session and a 500 ms interval between successive excitations, denoted as t1=0.05 ms and N=100. Consequently, 1000 images are acquired, corresponding to a total imaging duration of 50 ms at an effective frame rate of 20 kHz.

3.3. Agarose phantoms

The tissue-mimicking phantoms were fabricated by incorporating agarose powder (Biowest,CAS:9012-36-6) into hot water, followed by continuous heating of the mixture until the agarose was completely dissolved. Subsequently, a 1.6% intralipid (20%, CAS:68890-65-3) was added to enhance the scattering properties. The resulting mixture was then poured into plastic bowls with a radius of 12 cm and a depth of 6 cm to mold the phantoms. Four types of homogeneous phantoms with agarose concentrations of 0.6%, 0.8%, 1.2%, and 1.5% were made. Additionally, a two-sidedd mixed phantom with 0.6% and 1.2% agarose on either side was constructed.

3.4. Test on the rotary rheometer

To assess the validity of the laser profilometer elastography for measuring the shear elastic modulus of agarose phantoms, the shear elastic modulus of agarose samples with four concentrations of 0.6%, 0.8%, 1.2% and 1.5% was measured using the rotary rheometer. The plate rotary shear tests were performed with a rheometer (TA Instruments, Discovery HR-2), featuring a plate diameter of 25 mm, and a sample thickness of 3 mm. A strain of 0.5% was applied, and the storage modulus and loss modulus of samples were measured from 5 Hz to 50 Hz. The shear elastic modulus of the samples was calculated according to the Kelvin-Voigt model [21,39].

4. Results and discussion

Upon the acquisition of line profiles and imaging data, all datasets are subsequently processed utilizing customized MATLAB scripts.

4.1. Results from laser profilometer elastography

After collecting the profiles, missing values caused by scattering and underexposure in the profiles were filled using a median filter along the temporal axis. The laser profilometer measures the height of the phantom surface, which exhibits minor variations in height across different locations. Consequently, the baseline height for each position is subtracted along the spatial dimension.

Fig. 4(a) illustrates the spatiotemporal distribution of displacement under pulsed excitation with a sampling rate of 6.25 kHz for an agarose phantom with a concentration of 1.2%. The x-axis represents the temporal dimension, and the y-axis represents the travel distance from the initial reference point. The observation of multiple propagating waves is evident. Wave A denotes

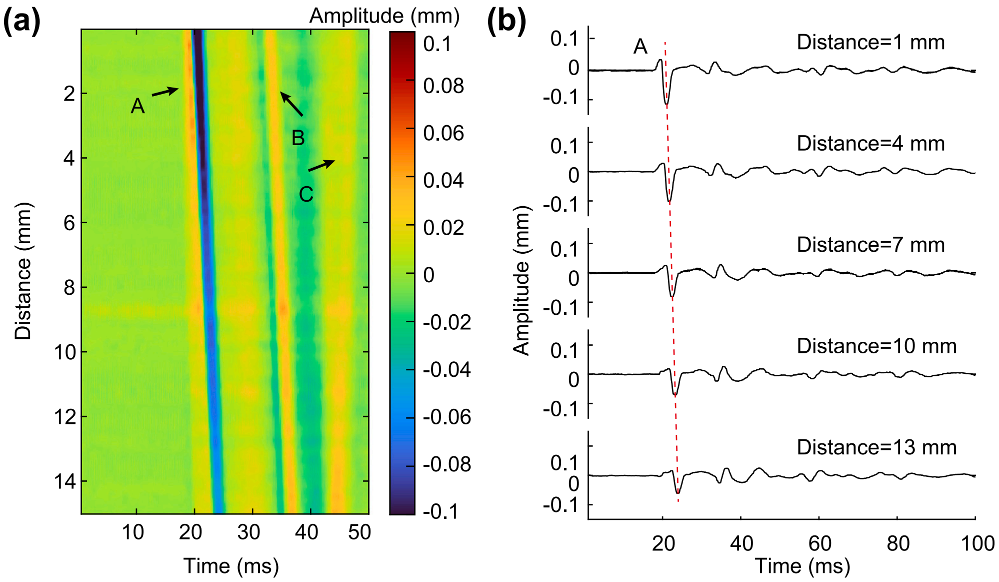

Fig. 4. Spatiotemporal distribution of surface wave under pulsed excitation. (a) An acquired time–space wavefield of surface waves. (b) Waveforms at specified locations, showing the approach used to measure the traveling time of surface waves. The red line indicates the wave valley, which can further be used to determine the surface wave velocity by using the traveling time and propagation distance. (For interpretation of the references to color in this figure legend, the reader is referred to the web version of this article.)

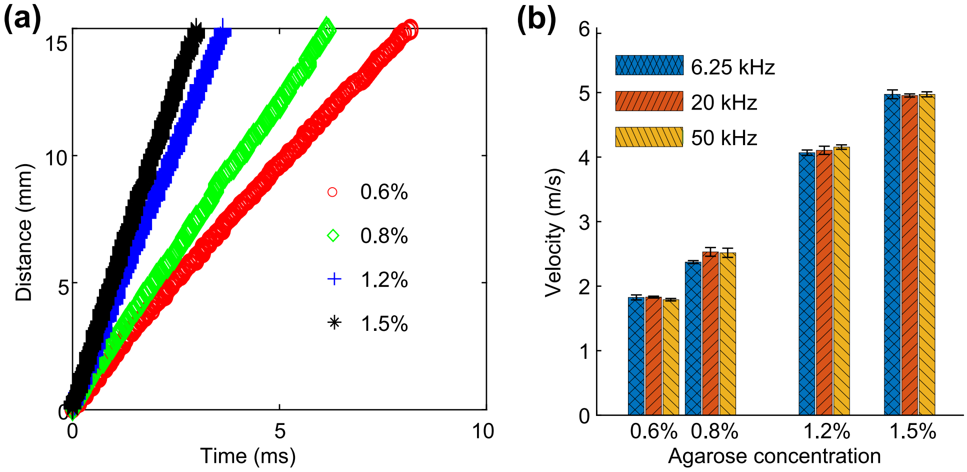

Fig. 5. Propagation velocity of the surface wave measured. (a) The travel distance of the surface wave exhibits a linear relationship with travel time on different phantoms. (b) Surface wave velocity measured of different phantoms using three distinct sampling rates.

the propagation of the primary surface wave, while waves B and C correspond to the secondary surface wave and the reflected wave, respectively. Fig. 4(b) shows the corresponding displacement waveform at typical positions, with the red line indicating the travel of the wave valley. The travel distance of the surface wave exhibits a linear relationship with travel time, which can further determine the surface wave propagation velocity. The surface wave gradually decays during propagation, causing the vibration amplitude to decrease from about 100 μm to 40 μm. Fluctuations of amplitude caused by the reflected waves at 100 ms can still be detected by the laser profilometer. The attenuation coefficient of the amplitude during surface wave propagation can also be used to calculate the viscoelasticity of the material [33]. However, amplitude attenuation is influenced by several factors including geometric spreading, scattering, and absorption. The velocity of compressive waves is significantly greater than that of surface waves. Under a single airpuff excitation, the primarily propagating surface waves and other reflected waves are spatiotemporally separated, and the amplitude of reflected waves is smaller, which is beneficial for identifying and calculating the propagation velocity of the surface wave.

For a particular wave peak, the arrived position is linear to the elapsed time, allowing the wave propagation velocity (group velocity) to be calculated using the time-of-flight algorithm. As shown in Fig. 5(a), with a sampling rate of 6.25 kHz, the travel

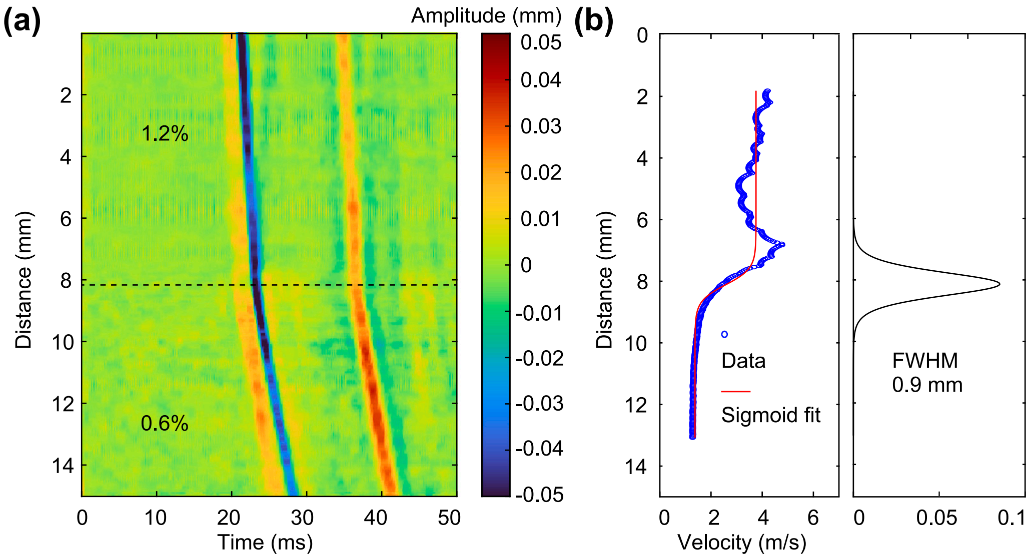

Fig. 6. Spatiotemporal distribution of surface wave under pulsed excitation on a two-sided phantom. (a) An acquired time–space wavefield of surface waves on a two-sided phantom. (b) Velocity distribution measured on the two-sided phantom and corresponding line edge response and point spread function.

distance of the surface wave varies linearly with travel time, and the velocity of the surface wave on agarose phantoms with different concentrations can be obtained through linear fitting. The propagation velocity of surface wave on a 0.6% concentration agarose phantom is the lowest, while the elasticity increases with concentration, which is consistent with previous literature reports [18,21]. The propagation velocities of surface waves in 0.6%, 0.8%, 1.2%, and 1.5% phantoms are 1.826 ± 0.039 m/s, 2.372 ± 0.023 m/s, 4.069 ± 0.041 m/s, and 4.973 ± 0.048 m/s respectively. In order to investigate the impact of sampling rate on the accuracy of elastic measurements, we conducted measurements on four phantoms with different concentrations utilizing three different sampling rates. The statistical results of three phantoms on each concentration are shown in Fig. 5(b). The propagation velocities of surface waves under the three different sampling rates at each concentration are in great agreement.

In order to investigate the impact of sampling speed on spatial resolution, we calculated the point spread function (PSF) of elastic measurements taken from non-uniform phantoms at various sampling rates. Fig. 6(a) shows the spatiotemporal distribution of surface wave propagation on a two-sided non-uniform phantom. The variation in the surface wave velocity across different concentrations of phantoms is evident. The propagation velocity of surface waves at different locations was calculated using a linear fit of the propagation line within a 2.2 mm (60 pixels) sliding window. As shown in Fig. 6(b), a sigmoid function is employed to fit the velocity distribution curve to get the line edge response curve (red curve in the left box). Subsequently, the derivative of this function is calculated to obtain the PSF curve (black curve in the right box). The full width at half maximum (FWHM) of the PSF curve at 6.25 kHz and 50 kHz is calculated to be 0.85 ± 0.12 mm and 0.76 ± 0.38 mm, respectively. The accuracy and spatial resolution of elastic measurements at a sampling rate of 6.25 kHz are comparable to those obtained at higher sampling rates of 20 kHz and 50 kHz. Configuring the profilometer to operate at a higher sampling rate, such as the maximum frequency, will result in a proportional decrease in exposure time. In scenarios where scattering of the phantom is minimal, the sensor exposure of the profilometer may be inadequate, thereby making contour extraction challenging or unsuccessful.

In contrast to the elastic measurement method using a stroboscope, as proposed by von Gierke [26], a laser profilometer was used in our study. The laser profilometer operates on the principle of triangulation measurement, which enhances its ability to detect displacement and offers superior motion sensitivity, achieving an accuracy of measurement at the micrometer level. This feature allows for the utilization of lower energy excitation. The advantages of employing low-energy excitation include: (1) the facilitation of non-contact excitation, which mitigates the risk of contamination of tissues or samples in both clinical and industrial contexts; (2) the ability to utilize a smaller excitation area, enabling higher excitation frequencies; (3) the prevention of sample damage, particularly in clinical settings where excessive excitation energy could harm the measured area, as well as in industrial applications where it may lead to the rupture of soft material samples; and (4) the reduction of displacements and the minimization of nonlinear effects within the sample.

High-efficiency frame rates can be achieved through the implementation of stroboscopic imaging timing. However, this approach requires multiple excitations and repeated sampling. We have previously studied two stroboscopic timing techniques to reduce the sampling rate requirements of the system [21,22]. One technique involves a delayed sampling timing technique combined with laser speckle imaging, which was proposed to track the surface wave at an equivalent frame rate of 20,000 frames/s. This facilitates the measurement of the viscoelastic properties of soft materials [22]. Additionally, we studied the laser speckle elastography method combining the aliasing effect, utilizing a camera operating at 10 frames/s to track the surface wave under continuous excitation at 400.5 Hz [21]. In this study, we also employed the stroboscopic timing method to obtain equivalent sampling rates of 20 kHz and

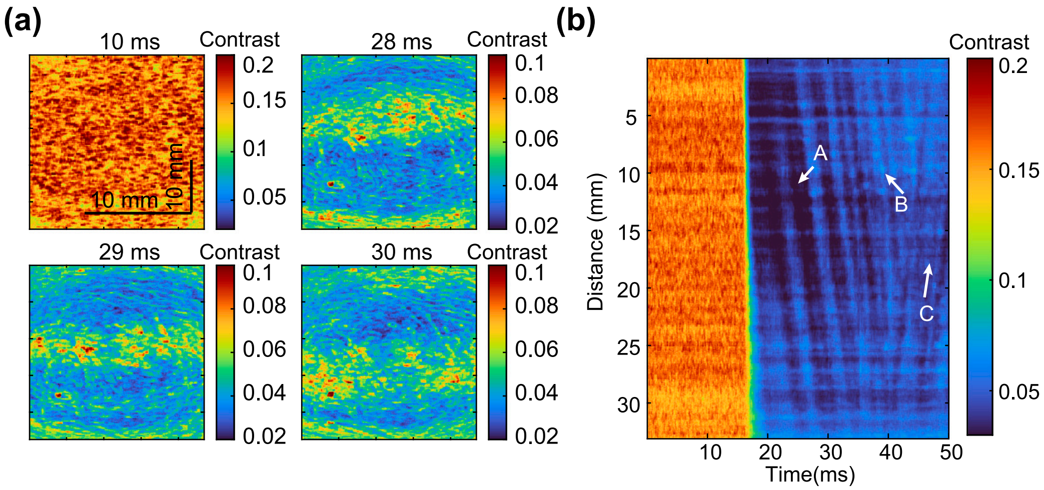

Fig. 7. Spatiotemporal distribution of surface wave propagation obtained by laser speckle elastography. (a) Speckle contrast imaging at different times. (b) An acquired time–space wavefield of surface waves.

50 kHz. The experimental findings indicate that the stroboscopic method requires multiple excitations and repeated sampling, which may contribute to an increase in detection errors. Several factors may contribute to this issue: (1) the use of multiple excitations or continuous excitations can lead to a more complex wave field due to the combination of various elastic wave modes and reflection waves. This complexity can adversely affect the precision of velocity calculations, whereas single-pulse excitation facilitates the spatiotemporal separation of waves with differing propagation speeds. (2) furthermore, the requirement for multiple excitations and sessions complicates the system's timing accuracy, potentially introducing instability due to random movements during the acquisition process, particularly in *in vivo* or online detection scenarios. (3) variations among multiple excitations can exacerbate errors within the detection system. In summary, The enhancement of system synchronization adds complexity, while interference from multiple excitations and the continuous reflection of wave fields can further complicate wave fields, thereby hindering accurate velocity calculations.

The excitation method employed in elastography presents a significant challenge within the field. Mechanical direct contact excitation methods, such as those utilizing piezoelectric crystals allow for more precise excitation of wave generation modes. Utilizing speaker-based contact excitation in elastography has proven to be both feasible and cost-effective. Previous researches conducted by our team have extensively utilized loudspeaker excitation for elastography [21,22]. However, it is important to note that speaker excitation necessitates direct contact with the sample being tested, which can lead to contamination in clinical applications and actual measurements. This issue is particularly problematic in scenarios, such as online monitoring of food production or the elastic assessment of traumatic tissues in medical settings. Consequently, this paper proposes using airpuff to facilitate non-contact excitation. The costs associated with non-contact excitation via airpuff are manageable, and such air sources are commonly employed in both production and medical environments, thereby eliminating the need for excessive hardware investments. Furthermore, portable inflatable pumps can be utilized to generate compressed air excitation at a relatively low cost.

4.2. Results from laser speckle elastography

The experiment setup and data processing method are discussed in our previous research on laser speckle elastography in detail [21,22]. The speckle contrast is first calculated with the spatial speckle contrast algorithm using a sliding window of 7 × 7 pixels size in accordance with Eq. (6). After reassembling 100 acquisitions in the correct chronological order, the time distribution of surface wave propagation is obtained. Fig. 7(a) shows speckle contrast imaging at time points of 10 ms, 28 ms, 29 ms, and 30 ms. At a time of 10 ms, the speckle contrast is high because there is no wave on the phantom. Both positive and negative vibration velocities of the surface wave will decrease the speckle contrast. The wave vibrations modulate the value of speckle contrast, resulting in a distinct propagation of waves in the vertical direction observed from 28 ms to 30 ms. Fig. 7(b) illustrates the spatiotemporal distribution of surface wave propagation obtained by laser speckle elastography. Prior to approximately 15 ms, the speckle contrast is about 0.2. The propagation of surface waves can be clearly observed, with different wave types denoted by the same letter in Fig. 4. The calculated propagation velocities of surface waves are 1.797 ± 0.303 m/s, 2.356 ± 0.180 m/s, 4.154 ± 0.275 m/s and 4.803 ± 0.401 m/s for 0.6%, 0.8%, 1.2%, and 1.5% concentration phantoms, respectively.

4.3. Compared to laser speckle elastography

Fig. 8(a) presents a comparative analysis of surface wave velocities, as measured by laser profilometer elastography and laser speckle elastography on agarose phantom with different concentrations. The error bars denote the standard deviation for three

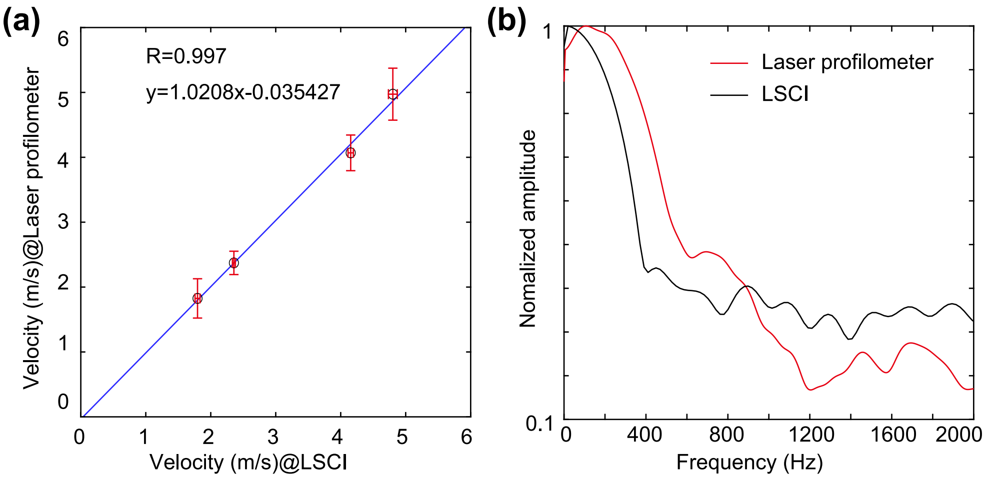

Fig. 8. Comparison between laser profilometer elastography and laser speckle elastography. (a) Scatter diagram of the propagation velocity and (b) frequency spectrum of the surface wave waveform measured using laser profilometer elastography and laser speckle elastography.

different samples at each concentration of agarose. The propagation velocities obtained by the two methods exhibited a strong agreement, with a correlation coefficient of 0.997. The errors in surface wave velocity measured by laser speckle elastography are greater than those measured by laser profilometer elastography. The possible reason is that laser speckle elastography utilized a stroboscopic imaging timing with 100 repeated excitations due to the limited frame rate of the camera. Initially, the errors associated with each airpuff excitation and the superimposition of waves in both spatial and temporal dimensions contribute to an increased imprecision in the measured wave field. Furthermore, LSCI cannot distinguish the direction of velocity, whereas laser profilometers are sensitive to axial displacement with both positive and negative directions. Therefore, it is advantageous for the laser profilometer to identify the primary surface wave by the spatiotemporal distribution of wave field detection.

Fig. 8(b) presents the frequency spectrum of the surface wave measured by both laser profilometer elastography (red curve) and laser speckle elastography (black curve). Laser profilometer elastography can detect a broader spectrum of the surface wave, which is more beneficial for viscoelasticity measurement by using elastic wave dispersion [2,22]. The speckle contrast represents statistical information of laser speckles, therefore multiple speckles need to be analyzed, resulting in the spatial averaging of the waveform to filter out high-frequency components. As demonstrated in our previous research [22], the spatiotemporal distribution of Rayleigh waves can be converted into the frequency–wavenumber domain through spectral transformation. This process facilitates the extraction of the phase velocity of Rayleigh waves across various frequencies, thereby elucidating the dispersion characteristics of Rayleigh waves, which can be utilized to assess the viscosity and elasticity of materials. It is important to note that the dispersion image of elastic waves is influenced by several factors, including viscosity and the finite volume of the sample. A viscoelastic measurement methodology utilizing a laser profilometer needs further investigation.

4.4. Compared to the rotary rheometer

As shown in Fig. 9(a), the storage modulus and loss modulus of 1.2% concentration agarose phantoms were measured, with the mean and standard deviation calculated from three samples at each concentration. The storage modulus remains relatively constant, exhibiting a slight increase in frequency. The loss modulus does not change with frequency, indicating that it is consistent with the pure elastic hypothesis. Fig. 9(b) shows the relationship between storage modulus and frequency for agarose samples with four different concentrations. It is evident that as the agarose concentration increases, the storage modulus also increases across all concentrations. The average storage modulus at different frequencies can be regarded as its shear elastic modulus [39].

The measurements of Rayleigh wave group velocity were transformed into shear elastic modulus utilizing Eq. (5). This conversion was conducted under the assumption of a density of 1000 $\mathrm{kg/m^3}$, and the premise that the phantom exhibits elasticity without surface wave dispersion, such that the group velocity is equivalent to the phase velocity [36]. As shown in Fig. 9(c), there is a strong correlation between the two methods with the correlation coefficient R = 0.997. There were slight deviations in the measured values between the two methods. This discrepancy may be attributed to the different frequencies employed in Rayleigh wave elastography and the rheometer, as the elastic properties of the medium are frequency-dependent. In Rayleigh wave elastography, the excitation frequency is approximately several hundred Hz, while the rheometer test operates at lower frequencies to ensure measurements remain within the linear viscoelastic range [18,21,39].

4.5. Influence of boundary conditions

Fig. 10(a) illustrates the relationship between the propagation velocities of surface waves and the thickness of the agarose phantom when subjected to airpuff excitation. The results indicate that at a thickness of approximately greater than 25 mm, the

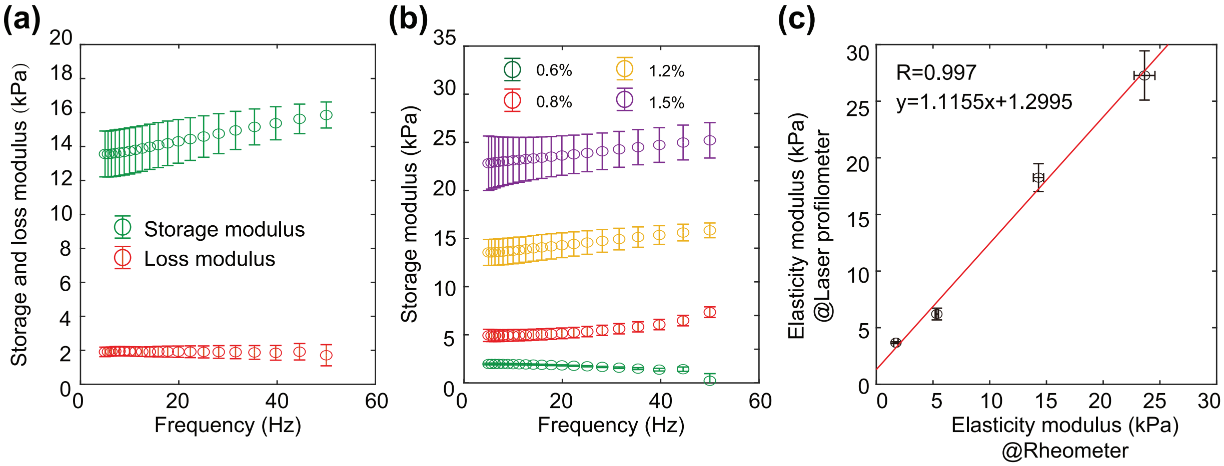

Fig. 9. Comparison between laser profilometer elastography and rotary rheometer. (a) The storage modulus and loss modulus of 1.2% agarose samples, (b) the storage modulus of four different concentrations of agarose samples, and (c) the scatter diagram of shear elastic modulus.

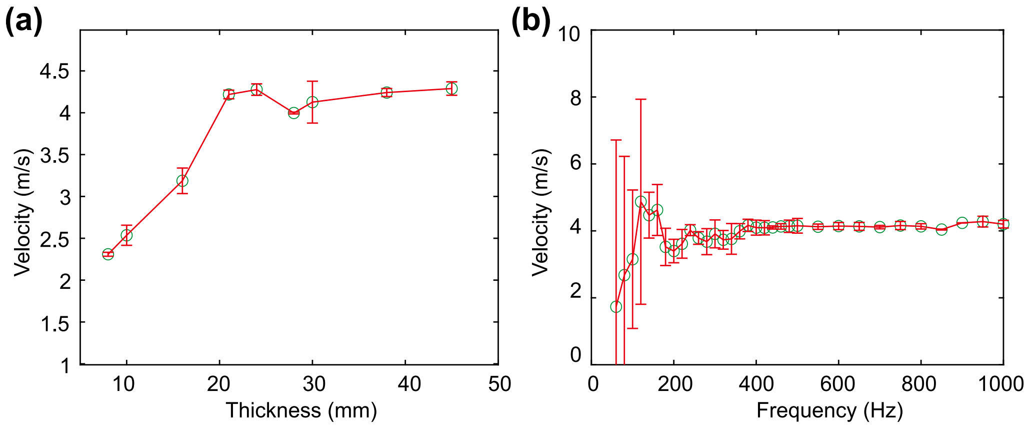

Fig. 10. Surface wave velocity changes as (a) the thickness of agarose phantoms under airpuff excitation and (b) the frequency of harmonic mechanical excitation using the audio speaker.

propagation velocity of the surface wave stabilizes, suggesting that variations in thickness have a minimal impact on the propagation velocity. Consequently, the sample can be considered as a semi-infinite medium. Fig. 10(b) shows the surface wave propagation velocities under different frequencies using the speaker mechanical excitation on an agarose phantom with a concentration of 1.2% and thickness of 30 mm. When the excitation frequency ranges from 400 Hz to 1000 Hz, the surface wave velocity remains unchanged, thereby fulfilling the criteria for a semi-infinite medium and can be classified as Rayleigh wave mode [2,3]. In the frequency range of 200 Hz to 400 Hz, there is a slight decrease in the surface wave velocity. When the frequency is below 200 Hz, considerable fluctuations in propagation velocity are observed, along with a noticeable reduction in the mean value. At low frequencies, the wavelength of the shear wave corresponds to the sample thickness, resulting in pronounced boundary effects [3]. Compared to harmonic excitation, pulse excitation encompasses a broad spectrum of frequency components, which complicates the classification of the elastic wave as a pure Rayleigh wave. However, the calculated group velocity remains relatively consistent with the phase velocity associated with Rayleigh wave propagation under high-frequency harmonic excitation. Consequently, it is reasonable to adopt the Rayleigh wave model for analysis.

In contrast, the airpuff excitation facilitates simple and noncontact excitation, it presents challenges in achieving high-frequency harmonic excitation. As illustrated in Fig. 8(b), the predominant frequency range of surface waves is below 800 Hz, with the propagation velocity of shear waves in biological soft tissues typically ranging from 1 m/s to 10 m/s. Assuming a surface wave velocity of 4 m/s and a frequency of 400 Hz, the resulting wavelength is approximately 10 mm. At lower frequencies, the idealized assumption of a semi-infinite medium is not valid, which may result in low-frequency surface waves not conforming to the Rayleigh wave mode. This is particularly relevant for rigid materials, such as aluminum plates, where the shear wave velocity is greater and the wavelength is longer. Consequently, the impact of the sample boundary on wave modes must be considered, and the Lamb wave model instead of the Rayleigh wave is often employed [6].

However, for soft material elastography, it is a prevalent practice to directly assume the Rayleigh wave mode, which may introduce tolerable inaccuracies in the results. It is important to note that biological tissues do not conform to a semi-infinite and homogeneous medium. For instance, the skin exhibits a layered structure, muscle tissue is anisotropic, and various structures, such as blood vessels, lymphatic vessels, and bones contribute to the complexity of the tissue composition. Additionally, the geometric configuration of a sample can lead to intricate boundary conditions. The creation of standard homogeneous samples is not feasible for elastic measurement *in vivo* or online, and accurately determining the specific mode of elastic waves presents challenges. Consequently, Elastography, including ultrasonic elastography and optical coherence elastography, relies on certain assumptions regarding the mode of the measured elastic wave [2,3,11,18]. Nonetheless, in soft materials, including soft tissues and hydrogels, the Poisson's ratio approaches 0.5, resulting in the velocity of Rayleigh waves being approximately 0.95 times that of shear waves. As frequency increases or sample thickness grows, the propagation velocities of Rayleigh waves and Lamb waves converge [32,40], thereby rendering the measurement error within acceptable limits.

In particular applications, the precise identification of the mode of the measured elastic wave can enhance the accuracy of the elastic measurements. For instance, in cornea elastography, it is commonly presumed that the elastic wave behaves as a Lamb wave [9]. In more general scenarios, spectral analysis techniques can be applied to extract the propagation characteristics of various wave modes. This approach is extensively utilized in shallow geophysics [34] and has potential applications in the study of biological tissues and soft materials.

5. Conclusion

In conclusion, this study first presented a novel noncontact elastic measurement method based on a laser profilometer with airpuff excitation. This method can track the propagation of surface waves under pulse airpuff excitation with a single excitation. The accuracy and resolution of the elastic measurements under 6.25 kHz in soft materials have been validated by comparison with equivalent high sampling rates of 20 kHz and 50 kHz. Compared to laser speckle elastography, laser profilometer elastography can detect a broader spectrum of surface wave waveforms and exhibits greater robustness in velocity measurements. The laser profilometer is simple in principle and is widely used in industry for high-precision measurement of material surface profiles. However, it has not been used for elastic measurement of the soft materials. The elastography method proposed in this article only requires the addition of an airpuff excitation to the existing laser profilometer. It has the potential to open a new application field for the laser profilometer. And it is hopefully to be used for tissue elasticity measurement in biomedical engineering, online elastic monitoring in the food industry, and elastic perception in robotics.

CRediT authorship contribution statement

Xiao Chen: Writing – original draft, Visualization, Validation, Methodology, Investigation, Funding acquisition, Formal analysis, Data curation, Conceptualization. **Yichu Chen:** Methodology, Investigation, Funding acquisition. **Wei Yu:** Writing – review & editing, Investigation. **Sanming Hu:** Writing – review & editing, Investigation. **Pengcheng Li:** Writing – review & editing, Methodology, Investigation, Funding acquisition.

Declaration of competing interest

The authors declare that they have no known competing financial interests or personal relationships that could have appeared to influence the work reported in this paper.

Acknowledgments

Funding: This work was supported by Hubei Provincial Natural Science Foundation of China (2024AFB453); Xianning Natural Science Foundation (2023ZRKX084); Hubei University of Science and Technology Doctoral Start-up Fund (BK202407). National Natural Science Foundation of China (NSFC) (82261138559, 62275095, 62305125), Hainan University Research Start-up Fund (KYQD(ZR)20072 and KYQD(ZR)22074); Hubei University of Science and Technology Research Development Fund(2024-25X11).

Data availability

Data will be made available on request.

References

[1] H.T. Banks, S. Hu, Z.R. Kenz, A brief review of elasticity and viscoelasticity for solids, Adv. Appl. Math. Mech. 3 (1) (2011) 1–51, http://dx.doi.org/10.4208/aamm.10-m1030.

[2] X. Feng, G.-Y. Li, S.-H. Yun, Ultra-wideband optical coherence elastography from acoustic to ultrasonic frequencies, Nat. Commun. 14 (1) (2023) 4949, http://dx.doi.org/10.1038/s41467-023-40625-y.

[3] N. Ghaderi, N. Hasheminejad, S. Sels, B. Ribbens, J. Dirckx, S. Vanlanduit, Soft material characterization through surface wave elastography using a laser doppler vibrometer, Mech. Syst. Signal Process. 224 (2025) 112037, http://dx.doi.org/10.1016/j.ymssp.2024.112037.

[4] B. Cai, T. Li, L. Bo, J. Li, R. Sullivan, C. Sun, W. Huberty, Z. Tian, Development of a piezo stack – laser doppler vibrometer sensing approach for characterizing shear wave dispersion and local viscoelastic property distributions, Mech. Syst. Signal Process. 214 (2024) 111389, http://dx.doi.org/10.1016/j.ymssp.2024.111389.

[5] M. Aktharuzzaman, S. Anwar, D. Borisov, J. He, Experimental full waveform inversion for elastic material characterization with accurate transducer modeling, Mech. Syst. Signal Process. 213 (2024) 111320, http://dx.doi.org/10.1016/j.ymssp.2024.111320.

[6] Z. Tian, S. Howden, Z. Ma, W. Xiao, L. Yu, Pulsed laser-scanning laser doppler vibrometer (PL-SLDV) phased arrays for damage detection in aluminum plates, Mech. Syst. Signal Process. 121 (2019) 158–170, http://dx.doi.org/10.1016/j.ymssp.2018.11.016.

[7] H. Yoon, J.-H. Kim, D. Sadat, A. Barrett, S.H. Ko, C. Dagdeviren, Decoding tissue biomechanics using conformable electronic devices, Nat. Rev. Mater. 10 (1) (2025) 14–27, http://dx.doi.org/10.1038/s41578-024-00729-3.

[8] P. Eliahoo, H. Setayesh, T. Hoffman, Y. Wu, S. Li, J.B. Treweek, Viscoelasticity in 3D cell culture and regenerative medicine: measurement techniques and biological relevance, ACS Mater. Au 4 (4) (2024) 354–384, http://dx.doi.org/10.1021/acsmaterialsau.3c00038.

[9] G.-Y. Li, X. Feng, S.-H. Yun, Simultaneous tensile and shear measurement of the human cornea in vivo using S0- and A0-wave optical coherence elastography, Acta Biomater. 175 (2024) 114–122, http://dx.doi.org/10.1016/j.actbio.2023.12.019.

[10] G. Schmidt, B.E. Bouma, N. Uribe-Patarroyo, Asynchronous, semi-reverberant elastography, Optica 11 (9) (2024) 1285–1294, http://dx.doi.org/10.1364/OPTICA.528507.

[11] H.-C. Liu, Y. Zeng, C. Gong, X. Chen, P. Kijanka, J. Zhang, Y. Genyk, H. Tchelepi, C. Wang, Q. Zhou, X. Zhao, Wearable bioadhesive ultrasound shear wave elastography, Sci. Adv. 10 (6) (2024) eadk8426, http://dx.doi.org/10.1126/sciadv.adk8426.

[12] M. Singh, F. Zvietcovich, C. Zevallos-Delgado, Y.S. Ambekar, S.R. Aglyamov, K.V. Larin, Whole embryo biomechanics with reverberant optical coherence elastography, Optica 11 (5) (2024) 686–692, http://dx.doi.org/10.1364/OPTICA.521367.

[13] H. Liu, D. Yang, R. Jia, W. Wang, J. Shang, Q. Liu, Y. Liang, Dynamic optical coherence elastography for skin burn assessment: a preliminary study on mice model, J. Biophoton. 17 (7) (2024) e202400028, http://dx.doi.org/10.1002/jbio.202400028.

[14] C. Wang, F. Fan, J. Ma, Z. Ma, X. Meng, J. Zhu, Optical coherence elastography under homolateral parallel acoustic radiation force excitation for ocular elasticity quantification, Opt. Lett. 49 (10) (2024) 2817–2820, http://dx.doi.org/10.1364/OL.523215.

[15] W. Moon, X. Feng, G.-Y. Li, S.-H. Yun, High-frequency optical coherence elastography for gingival tissue characterization: Variability in stiffness and response to physiological conditions, Biomater. Res. 28 (2024) 0044, http://dx.doi.org/10.34133/bmr.0044.

[16] Y. Liu, R. Shi, G. Li, M. Sun, Photoacoustic elastography based on laser-excited shear wave, J. Innov. Opt. Heal. Sci. 17 (3) (2024) 2350031, http://dx.doi.org/10.1142/S1793545823500311.

[17] S. Paul, S. Kumar Yadav, M. Suheshkumar Singh, Surface-wave-induced photoacoustic elastography in the feasibility study of tissue biomechanical properties, IEEE Trans. Instrum. Meas. 73 (2024) 1–10, http://dx.doi.org/10.1109/TIM.2024.3398128.

[18] A. Singh, F. Pati, R. John, Quantifying viscosity and elasticity using holographic imaging by Rayleigh wave dispersion, Opt. Lett. 47 (9) (2022) 2214–2217, http://dx.doi.org/10.1364/OL.451464.

[19] N. Leartprapun, Z. Zeng, Z. Hajjarian, V. Bossuyt, S.K. Nadkarni, Laser speckle rheological microscopy reveals wideband viscoelastic spectra of biological tissues, Sci. Adv. 10 (19) (2024) eadl1586, http://dx.doi.org/10.1126/sciadv.adl1586.

[20] P.-Y. Chao, P.-C. Li, Laser-speckle-contrast projection tomography for three-dimensional shear wave imaging, Opt. Lett. 44 (19) (2019) 4809–4812, http://dx.doi.org/10.1364/OL.44.004809.

[21] X. Chen, J. Lu, P. Li, Elastography with low-frame-rate laser speckle contrast imaging using the aliasing effect, Opt. Lett. 43 (12) (2018) 2811–2814, http://dx.doi.org/10.1364/OL.43.002811.

[22] X. Chen, Y. Wang, J. Lu, P. Li, Simultaneous viscosity and elasticity measurement using laser speckle contrast imaging, Opt. Lett. 43 (7) (2018) 1582–1585, http://dx.doi.org/10.1364/OL.43.001582.

[23] Z. Wang, J. Liu, C. Fang, K. Wang, L. Wang, Z. Wu, Nondestructive measurements of elastic constants of thin rods based on guided waves, Mech. Syst. Signal Process. 170 (2022) 108842, http://dx.doi.org/10.1016/j.ymssp.2022.108842.

[24] C. Song, W. He, J. Feng, M.D. Twa, Y. Huang, J. Xu, J. Qin, L. An, X. Wei, G. Lan, Dual-channel air-pulse optical coherence elastography for frequency-response analysis, Biomed. Opt. Express 15 (5) (2024) 3301–3316, http://dx.doi.org/10.1364/BOE.520551.

[25] S. Rothberg, M. Allen, P. Castellini, D. Di Maio, J. Dirckx, D. Ewins, B. Halkon, P. Muyshondt, N. Paone, T. Ryan, H. Steger, E. Tomasini, S. Vanlanduit, J. Vignola, An international review of laser doppler vibrometry: making light work of vibration measurement, Opt. Lasers Eng. 99 (2017) 11–22, http://dx.doi.org/10.1016/j.optlaseng.2016.10.023.

[26] H.E. von Gierke, H.L. Oestreicher, E.K. Franke, H.O. Parrack, W.W. von Wittern, Physics of vibrations in living tissues, J. Appl. Physiol. 4 (12) (1952) 886–900, http://dx.doi.org/10.1152/jappl.1952.4.12.886.

[27] M. Qu, Q. Guo, L.I. Escano, J. Yuan, S.M.H. Hojjatzadeh, S.J. Clark, K. Fezzaa, T. Sun, L. Chen, Controlling melt flow by nanoparticles to eliminate surface wave induced surface fluctuation, Addit. Manuf. 59 (2022) 103081, http://dx.doi.org/10.1016/j.addma.2022.103081.

[28] V.I. Moreno-Oliva, O. Flores-Diaz, E. Román-Hernández, M. Campos-García, E. Campos-Mercado, J.R. Dorrego-Portela, Q. Hernandez-Escobedo, J.A. Franco, A.-J. Perea-Moreno, A.A. García, Vibration measurement using laser triangulation for applications in wind turbine blades, Symmetry 13 (6) (2021) 1017, http://dx.doi.org/10.3390/sym13061017.

[29] D. Ding, W. Ding, R. Huang, Y. Fu, F. Xu, Research progress of laser triangulation on-machine measurement technology for complex surface: a review, Measurement 216 (2023) 113001, http://dx.doi.org/10.1016/j.measurement.2023.113001.

[30] T. Royston, H. Mansy, R. Sandler, Excitation and propagation of surface waves on a viscoelastic half-space with application to medical diagnosis, J. Acoust. Soc. Am. 106 (6) (1999) 3678–3686.

[31] T.J. Royston, Z. Dai, R. Chaunsali, Y. Liu, Y. Peng, R.L. Magin, Estimating material viscoelastic properties based on surface wave measurements: A comparison of techniques and modeling assumptions, J. Acoust. Soc. Am. 130 (6) (2011) 4126–4138.

[32] I.Z. Nenadic, M.W. Urban, S. Aristizabal, S.A. Mitchell, T.C. Humphrey, J.F. Greenleaf, On Lamb and Rayleigh wave convergence in viscoelastic tissues, Phys. Med. Biol. 56 (20) (2011) 6723.

[33] S.J. Kirkpatrick, D.D. Duncan, L. Fang, Low-frequency surface wave propagation and the viscoelastic behavior of porcine skin, J. Biomed. Opt. 9 (6) (2004) 1311–1319.

[34] C. Strobbia, S. Foti, Multi-offset phase analysis of surface wave data (MOPA), J. Appl. Geophys. 59 (4) (2006) 300–313.

[35] L. Yu, Z. Tian, Guided wave phased array beamforming and imaging in composite plates, Ultrasonics 68 (2016) 43–53, http://dx.doi.org/10.1016/j.ultras.2016.02.001.

[36] N.C. Rouze, A. Caenen, K.R. Nightingale, Phase and group velocities for shear wave propagation in an incompressible, hyperelastic material with uniaxial stretch, Phys. Med. Biol. 67 (9) (2022) 095015.
[37] X. Zhang, Identification of the Rayleigh surface waves for estimation of viscoelasticity using the surface wave elastography technique, J. Acoust. Soc. Am. 140 (5) (2016) 3619–3622.
[38] X. Zhang, J.F. Greenleaf, Estimation of tissue's elasticity with surface wave speed, J. Acoust. Soc. Am. 122 (5) (2007) 2522–2525.
[39] Y. Zhu, C. Dong, Y. Yin, X. Chen, Y. Guo, Y. Zheng, Y. Shen, T. Wang, X. Zhang, S. Chen, The role of viscosity estimation for oil-in-gelatin phantom in shear wave based ultrasound elastography, Ultrasound Med. Biol. 41 (2) (2015) 601–609.
[40] I.Z. Nenadic, M.W. Urban, M. Bernal, J.F. Greenleaf, Phase velocities and attenuations of shear, Lamb, and Rayleigh waves in plate-like tissues submerged in a fluid (L), J. Acoust. Soc. Am. 130 (6) (2011) 3549–3552.